Holographic Photopolymerization-Induced Phase Separation in Reference to the Phase Diagram of a Mixture of Photocurable Monomer and Nematic Liquid Crystal

Scott Meng,[†] Thein Kyu,*[,†] Lalgudi V. Natarajan,[‡] Vincent P. Tondiglia,[‡] Richard L. Sutherland,[‡] and Timothy J. Bunning[§]

Department of Polymer Engineering, University of Akron, Akron, Ohio 44325; Science Applications International Corporation, Dayton, Ohio 45431; and Air Force Research Laboratory, Materials and Manufacturing Directorate, Wright-Patterson Air Force Base, Ohio 45433

Received September 15, 2004; Revised Manuscript Received April 4, 2005

ABSTRACT: Theoretical investigation on pattern photopolymerization has been undertaken in various coexistence regions of a mixture of photocurable monomer and nematic liquid crystal. The phase diagram of the mixtures is constructed in accordance with a combined Flory−Huggins (FH) free energy of isotropic mixing and the Maier−Saupe (MS) free energy of nematic ordering. The pattern formation dynamics of holographic photopolymerization has been explored in conjunction with the phase diagram of the starting mixture of monomer and nematic liquid crystal. To mimic the evolution of holographic structure, the combined FH and MS free energy is incorporated into the time-dependent Ginzburg−Landau (model C) equations coupled with the photopolymerization kinetic equation. The morphology evolution and mechanisms have been investigated in relation to the situations whether the system should remain in the single phase after photopolymerization or be thrust into the two-phase region. Of particular significance is that the diffraction efficiency (DE) of gratings, a key property in electrooptical applications, can be monitored in-situ during photopatterning. In the gratings of inhomogeneous structures, scattering occurs due to the interparticle interference, which needs to be accounted for in the evaluation of the DE. A fast Fourier transformation (FFT) technique of the emerging morphological domains of the holographic polymer dispersed liquid crystals uniquely provides the simultaneous determination of the diffraction peaks from the holographic layers as well as scattering from the internal LC domains; thereby, the DE correction is feasible. The simulated patterns and the trends of diffraction efficiency evolution are compared with experimental observations.

Introduction

As is well-known, holographic polymer dispersed liquid crystal (H-PDLC) is a unique composite material possessing periodic alignment of polymer and liquid crystal in layers.[1,2] Nowadays, it has been realized that the H-PDLC likewise falls into the category of one-dimensional photonic crystals, which covers a much broader class of periodic structural materials that is not limited to liquid crystal and polymeric materials.[3] The most important feature of photonic crystals is that these materials possess the photonic band-gap (PBG) structures, through which propagation of light of a designated frequency range is prohibited.[4,5] These one-/multidimensional periodic structures open the door to a variety of potential applications ranging from beam steering, optical gauge, and electrooptical communication devices as well as information storage media.[6,7]

A general approach in fabricating H-PDLC is via photopolymerization-induced phase separation. This technique involves two beams reflected to the sample surface at a certain angle. By virtue of the constructive and destructive interference of the incident beams, high-intensity and low-intensity regions are created in the sample.[8] Alternatively, four waves may be employed to generate three-dimensional photonic structures. The pattern photopolymerization approach is advantageous in its superfast processing time, chemical versatility, and reproducibility, making it a possible candidate for holographic applications.[9]

One of the most important factors that determine the electrooptical performance of H-PDLC is its morphology. The morphology of H-PDLC has been characterized by a number of methods such as scanning electron microscopy, transmission electron microscopy, and atomic force microscopy. So far, two distinct morphologies have been observed experimentally.[10] The first is the "Swiss cheese" type with phase-separated liquid crystal droplets layers alternating with cross-linked polymer layers. The second is the "spongelike" type with interconnected bicontinuous liquid crystal layers alternating with cross-linked polymer layers. Within the highly cross-linked polymer regions, sizable amount of liquid crystals are found to be trapped. Several variables controlling the emerged morphology have been investigated, including monomer functionality, monomer type, liquid crystal content, starting temperature, among others.[10,11]

Although the photopatterning process in the neat photoreactive monomers has been calculated numerically on the basis of the reaction−diffusion equation,[12] there is limited theoretical effort in elucidating the emergence of phase-separated domains in the confined stratified regions. In the literature, a conventional reaction−diffusion equation has been applied to the binary system,[13,14] but the issues of phase separation and nematic ordering of LC were not addressed. Recently, Sutherland et al.[15] have presented a thermodynamic equilibrium approach to account for phase sepa-

[†] University of Akron.
[‡] Science Applications International Corporation.
[§] Air Force Research Laboratory.
* Corresponding author: e-mail tkyu@uakron.edu.

10.1021/ma0480906 CCC: $30.25
Published on Web 05/07/2005

ration and nematic ordering of LC processes individually by incorporating it into the general reaction−diffusion equation.[15] Subsequently, one-dimensional solution was deduced, from which the diffraction efficiency evolution was computed on the basis of the dielectric contrasts of the stratified layers. Their work is probably the first to link the equilibrium structure with the electrooptical switching characteristics of H-PDLC.

In the present work, we have performed a two-dimensional coarse-grain modeling based on the time-dependent Ginzburg−Landau (TDGL) equation by incorporating the combined Flory−Huggins (FH)/Maier−Saupe (MS) free energy representing phase separation and nematic ordering, respectively. The major goal is to elucidate the diverse morphologies for the H-PDLC films formed in relation to the phase diagrams of the nematic liquid crystal and photoreactive monomer mixture. The present paper is an extension of Sutherland's approach,[15] in that the phase separation and nematic ordering processes have been treated in a coupled fashion, and thus the emerged morphological details inside the alternating stripes can be captured. Subsequently, we have calculated the time progression of the diffraction efficiency (DE) using the approach of fast Fourier transformation (FFT) of the emerging H-PDLC domains. One advantage of the FFT approach is that the DE thus evaluated is the statistical average of the local variation of the dielectric constants corresponding to the local concentration fluctuations; therefore, any contribution from the local morphological details as well as changes in the concentration and director orientation profiles to the DE can be accounted for in the Fourier space.

Modeling the Phase Equilibrium of Polymer/LC Mixtures. In general, the total free energy of the polymer/LC mixture is composed of the free energy from isotropic−isotropic phase separation and the free energy from nematic ordering. The local free energy density of isotropic mixing may be described in accordance with the Flory−Huggins model[16,17]

$$g^{\mathrm{i}} = \phi_{\mathrm{LC}} \ln \phi_{\mathrm{LC}}/r_{\mathrm{LC}} + (1 - \phi_{\mathrm{LC}}) \ln \phi_{\mathrm{LC}}/r_{\mathrm{m}} + \chi\phi_{\mathrm{LC}}(1 - \phi_{\mathrm{LC}}) \quad (1)$$

where g^{i} stands for the isotropic local free energy density of mixing. ϕ_{LC} represents the liquid crystal volume fraction, with r_{m} and r_{LC} the respective statistical chain segment lengths of polymer and liquid crystal molecules which are taken as unity at the onset of polymerization. χ is the Flory−Huggins interaction parameter which may be expressed as $\chi = A + B/T$, where A and B are constants and T is the system's temperature.

The local free energy density of nematic ordering may be described by the Maier−Saupe theory as[18]

$$g^{\mathrm{n}} = \frac{1}{r_{\mathrm{LC}}}\left(-\phi_{\mathrm{LC}} \ln z + \frac{1}{2}\nu{\phi_{\mathrm{LC}}}^2 s^2\right) \quad (2)$$

where g^{n} symbolizes the anisotropic free energy from nematic ordering. ν is the nematic interaction parameter having the form $\nu = 4.541T_{\mathrm{NI}}/T$, in which T_{NI} is the liquid crystal nematic−isotropic transition temperature and z is the partition function defined as

$$z = \int_0^1 \exp\left[\frac{\nu\phi_{\mathrm{LC}}s}{2}(3x^2 - 1)\right] \mathrm{d}x \quad (3)$$

where s is the nematic orientation order parameter given by

$$s = \frac{\int_0^1 \frac{1}{2}(3x^2 - 1) \exp\left[\frac{\nu\phi_{\mathrm{LC}}s}{2}(3x^2 - 1)\right] \mathrm{d}x}{z} \quad (4)$$

with $x = \cos\theta$, θ being the angle between the LC director and the reference axis.

Phase Diagram Establishment. One of the important criteria for the phase equilibrium is that the chemical potential (μ) of each component of the system must be balanced in each phase. To determine the coexistence points of isotropic−isotropic phase separation in a binary fluid, one obtains

$$\mu_1({\phi_i}^{\alpha}) = \mu_1({\phi_i}^{\beta}) \quad \text{and} \quad \mu_2({\phi_i}^{\alpha}) = \mu_2({\phi_i}^{\beta}) \quad (5)$$

Regarding the nematic−isotropic phase separation in a binary system, the coexistence points can be determined as

$$\mu_1({\phi_{\mathrm{n}}}^{\alpha},s) = \mu_1({\phi_{\mathrm{i}}}^{\beta},0) \quad \text{and} \quad \mu_2({\phi_{\mathrm{n}}}^{\alpha},s) = \mu_2({\phi_{\mathrm{i}}}^{\beta},0) \quad (6)$$

where the superscripts α and β refer to respective coexisting phase, the subscripts 1 and 2 represent individual components of the system, and the subscripts i and n denote the isotropic and nematic states. The equilibrium solutions at different temperatures can be obtained by using a double-tangent method,[19] whereas the spinodal point can be determined by equating the second derivative of free energy to zero. In the case of isotropic-isotropic demixing, there are two roots. In the case of nematic−isotropic demixing, there exist at most three solutions.

Modeling of Pattern Photopolymerization Dynamics in Polymer and Nematic Liquid Crystal Mixtures. The dynamics of pattern photopolymerization in mixtures of emerging polymer and nematic liquid crystal may be modeled by means of the time-dependent Ginzburg−Landau equations (TDGL, model C) with a conserved compositional order parameter ϕ and a non-conserved orientation order parameter s coupled with photopolymerization reaction kinetics.[20] The spatiotemporal change of the LC concentration may be monitored via

$$\frac{\partial\phi_{\mathrm{LC}}(\vec{r},t)}{\partial t} = \nabla\cdot\left[\Lambda\nabla\left(\frac{\delta G}{\delta\phi_{\mathrm{LC}}}\right)\right] \quad (7)$$

where $(\delta G/\delta\phi_{\mathrm{LC}})$ is the functional derivative of the total free energy with respect to the LC concentration representing the chemical potential of LC phase. Photopolymerization is triggered by the free radical photoinitiation and proceeds through the free-radical or the condensation reaction route depending on the type of photoinitiators and the functional groups of the monomers utilized. In free-radical polymerization, although molecular weight of polymers can rapidly reach a relatively high level, remaining sizable unreacted monomers, unlike the case of condensation polymerization, where almost all monomers are sequentially converted into dimers, tetramers, and oligomers in the early stage. Therefore, the depletion rate of the monomer concentration is different for different polymerization reactions. Free radical photopolymerization in a layer pattern may be described as

$$\frac{\partial \phi_m(\vec{r},t)}{\partial t} = \nabla\cdot\left[\Lambda\nabla\left(\frac{\delta G}{\delta \phi_m}\right)\right] - k\left[1 + v\cos\left(\frac{2\pi x}{L}N_x\right)\right]\phi_m \quad (8)$$

The emerging polymer concentration may then be expressed as

$$\frac{\partial \phi_p(\vec{r},t)}{\partial t} = \nabla\left[\Lambda\nabla\left(\frac{\delta G}{\delta \phi_p}\right)\right] + k\left[1 + v\cos\left(\frac{2\pi x}{L}N_x\right)\right]\phi_m \quad (9)$$

with $k = (k_p/k_t^{1/2})(\Phi I_a)$, k representing the apparent reaction kinetic constant, in which k_p and k_t represent the individual reaction kinetic constants for propagation and termination, respectively. Φ is referred to as the quantum yield for initiation. I_a corresponds to the absorbed light intensity, and v is the controlling factor of the amplitude of light wave. N_x stands for the number of gratings, and L indicates the length of relevant H-PDLC square grid. The subscripts LC, m, p, and s signify the liquid crystal, monomer, emerging polymer concentration, and liquid crystal orientation, respectively.

The orientational ordering of LC is given as

$$\frac{\partial s(\vec{r},t)}{\partial t} = -R_s\left(\frac{\delta G}{\delta s}\right) \quad (10)$$

R_s is related to the rotational mobility of the liquid crystal director, which is inversely proportional to the drag force or viscosity. The local free energy in the TDGL model C equations can be represented by the isotropic free energy of mixing given by the Flory–Huggins model (g^i) and nematic ordering free energy given by the Maier–Saupe theory (g^n) mentioned earlier in the phase diagram establishment section. The total free energy of the system G is defined as

$$G = \int_V (g^i + g^n + \kappa_\phi|\nabla\phi|^2 + \kappa_s|\nabla s|^2)\,dV \quad (11)$$

where κ_ϕ is the interfacial gradient coefficient of concentration which is associated with the segmental characteristic lengths and local concentrations. For an asymmetric system, it can be written as

$$\kappa_\phi = \frac{1}{36}\left[\frac{a_1^2}{\phi_{LC}} + \frac{a_2^2}{\phi_m}\right] \quad (12)$$

where a_1 and a_2 are the characteristic lengths of segments of LC and monomer, respectively. κ_s represents the gradient coefficient of orientation order parameter which is taken as constant in the simulation for simplicity.

The mutual diffusion coefficient Λ satisfies the Onsager reciprocity such that

$$\Lambda = \frac{\Lambda_m\Lambda_{LC}}{\Lambda_m + \Lambda_{LC}} \quad (13)$$

By nature of the cross-linking reaction, the mutual diffusion is essentially between the residual monomer and LC as the emerging polymer chains are fixed at the chemical junction. Hence, the first term (diffusion term) on the right-hand side of eq 9 may be eliminated. The respective diffusivity of monomer and LC can be related to the self-diffusion coefficients of monomer and LC as $\Lambda_m = D_m\phi_m r_m$ and $\Lambda_{LC} = D_{LC}\phi_{LC}r_{LC}$.

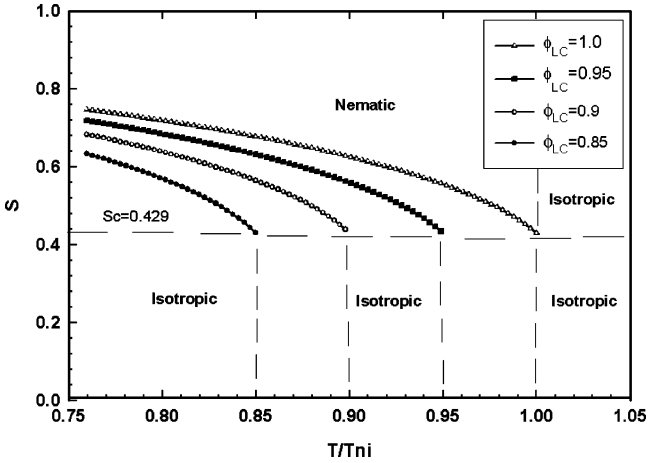

Figure 1. Plots of orientation order parameter s vs ratio of different temperatures over T_{NI} at various liquid crystal concentrations.

If the emerging polymers were completely miscible with the residual monomers, the system may be simplified as a pseudo-two-phase system with one component being liquid crystal and the other component being the homogeneous mixture of emerging polymer and residual monomer. With this simplification, the temporal progression (snapshot) of the phase diagram movement may be monitored as a function of the progression of the photopolymerization.

A hypothetical phase diagram was constructed by solving eqs 1–6 self-consistently. The numerical solutions of these equations afford the dynamics of H-PDLC formation. The spatiotemporal growth of the structure has been simulated on a 128 × 128 grid by employing a finite central difference method for the spatial step and explicit forward difference method for the time step under periodic boundary conditions. To ensure the stability of the simulation, various grid sizes and time steps have been utilized. The reference system for simulation is a mixture of multifunctional photoreactive monomer (e.g., pentacrylate) and low molar nematic liquid crystal (e.g., cyanobiphenyl derivatives). The diffusion coefficients for simulation are chosen within the experimental range of the diffusion coefficients for liquid crystal (10^{-7}–10^{-8} cm^2/s) and for the multifunctional acrylic monomer (10^{-10}–10^{-11} cm^2/s).

Results and Discussion

It is instructive to examine the behavior of the orientation order parameter s in relation to the nematic–isotropic phase transition prior to the establishment of any phase diagram. Figure 1 exhibits a plot of orientation order parameter s as a function of the reduced temperature, i.e., the ratio of temperature of interest vs nematic isotropic transition temperature at various volume fractions of liquid crystal. In the pure LC, the value of s decreases discontinuously at a transition temperature. This discontinuous transition is regarded as the nematic–isotropic transition temperature, T_{NI}. The same trend can be discerned for the blends of monomer and LC. The reduction of the T_{NI} with increasing monomer concentration may be attributed to the plasticization effect caused by the miscibility between the constituents. For a given volume fraction of liquid crystal, there exists a universal critical order parameter s_c. Below s_c, the order parameter s drops discontinuously to zero, characteristic of a first-order phase transition for the nematic ordering.

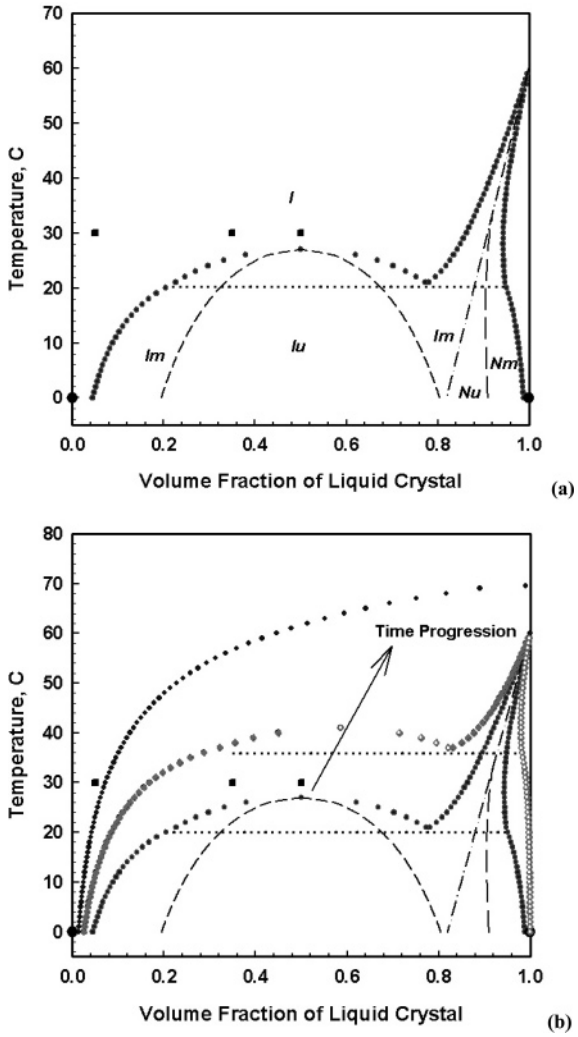

Figure 2. A hypothetical phase diagram of monomer and nematic liquid crystal mixtures (a). Illustrations of hypothetical phase diagram evolution as a function of time during the photopolymerization (b).

Figure 2a depicts a hypothetical phase diagram of polymer/LC mixtures before the initiation of photopolymerization calculated based on the following conditions: $r_m = r_{LC} = 1$ and the critical temperature $T_c = 27$ °C. The constant A in the Flory–Huggins interaction parameter is set arbitrarily as -10, which in turn yields $B = 3600$ from the relationship $\chi_c = A + B/T_c$, where T_c and χ_c are the critical temperature and interaction parameter, respectively. Alternatively, χ_c can be estimated via the critical condition

$$\chi_c = \frac{(\sqrt{r_{LC}} + \sqrt{r_m})^2}{2r_{LC}r_m} \tag{14}$$

The nematic–isotropic transition temperature is taken as that of the reference nematic liquid crystal: $T_{NI} = 60$ °C. Therefore, the nematic interaction parameter is determined in accordance with $\nu = 4.541T_{NI}/T$. The dotted thin line parallel to the x-axis in Figure 2a is the peritectic line, which signifies the isotropic–isotropic phase separation region and liquid–nematic phase separation region. In Figure 2a,b, the notations I and N stand for isotropic and nematic state, respectively, whereas subscripts m and u denote the metastable and unstable regions, respectively. The progression of phase diagram with time is plotted in Figure 2b. As illustrated in the figure, the solid square dots above the coexistence curve represent three systems that are at the same temperature but compositionally different. The subsequent simulations are meant to check the dynamical growth behavior of these systems at these three concentrations as the starting conditions.

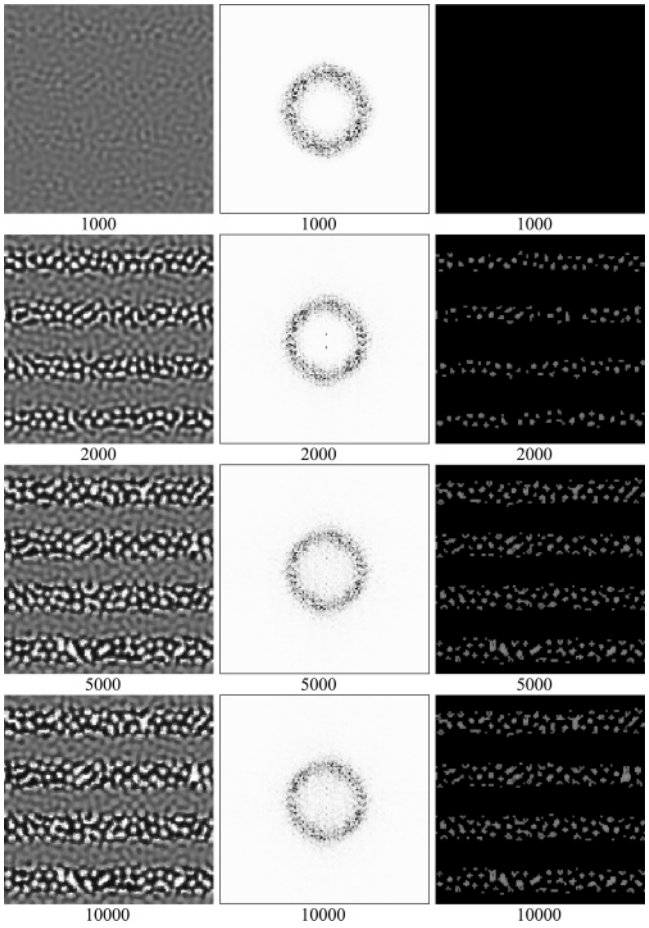

Figure 3. Simulated spatiotemporal growth of concentration order parameter (left array), Fourier transform patterns (middle array), and orientation order parameter (right array) under two-wave interference pattern photopolymerization for liquid crystal and photoreactive monomer mixed at the ratio of 50/50.

Figure 3 illustrates the simulated spatiotemporal growth of the LC concentration order parameter via the two-wave interference pattern photopolymerization technique under the following conditions: $\phi_{LC} = 0.5$ and $T = 30$ °C. Other parameters used in the simulation are the same as the ones for the phase diagram calculation along with the kinetic parameters: $k = 1 \times 10^{-3}$, $D_m = 0.01$, $D_{LC} = 2$, $R_s = 0.1$, $\kappa_\phi = 0.6$, and $\kappa_s = 0.1$. Once photopolymerization begins, the phase diagram of the LC/monomer mixture asymmetrically shifts upward by virtue of the increase in the molecular weight of the emerging polymer. The initial reaction temperature in the single-phase is pushed into an unstable region as the immiscible gap expands. Subsequently, macroscopic phase separation takes place, driving the system into the phase-separated domains that are liquid crystal-rich and liquid crystal-lean. Photocurable monomers tend to diffuse into the high-intensity region where the photopolymerization is most efficient. On the other hand, liquid crystals diffuse into the region where the intensity is low, thereby forming a liquid-crystal-rich phase.

It is evident from Figure 3 that the morphology development in the 50/50 LC/monomer mixtures first started with phase separation around 1000 time steps. The structure is reminiscent of a bicontinuous spinodal decomposition type, although it is by no means a proof. At 2000 time steps, a distinct morphology was discerned, in which the liquid crystal domains preferentially resided in the low light intensity region. In the high intensity regions, some liquid crystals might be trapped within the cross-linked polymer network. The entrapped LC molecules in this network retain some mobility that allows LC molecules to diffuse in and out of the network, although the polymer chains in the high intensity region are practically tied at the chemical junctions. Structures in the low intensity region of light coalesce into larger domain sizes. From 5000 time steps to 10 000 time steps, the system seemingly reaches the final stage asymptotically.

Among the Fourier transform patterns of the concentration order parameter in Figure 3 (middle column), a scattering halo was observed initially around 1000 time steps. This scattering halo is initially weak and fuzzy. At 2000 time steps, a pair of diffraction spots becomes discernible inside the scattering ring. The scattering halo gradually shrinks and concurrently intensifies. At 5000 time steps, the diffraction spots become blurred. The appearance of these diffraction spots is a clear indication of a grating formation in contrast to the scattering halo resulting from the interparticle interference of the phase-separated domains within each stripe. The shrinkage and intensification of the scattering ring indicate the growth of the average domain size. The competition between the scattering halo and diffraction peaks plays a crucial role in the determination of electrooptical properties of H-PDLC such as the diffraction efficiency (DE). Generally speaking, a suppressed scattering halo with intense diffraction spots is preferred for the DE optimization.

The spatiotemporal growth of the LC orientation order parameter under the two-wave interference pattern photopolymerization is depicted in the right column of Figure 3. No identifiable texture is noticed in the orientation domains prior to 1000 time steps, implying that the structure development in the orientation field lagged behind that of the concentration field. Subsequently, anisotropic LC domains developed within the alternating stripes. In the high-intensity region, there is no nematic ordering of LC because the LC molecules trapped in the network may be below the threshold concentration for nematic ordering to take place.

Figure 4 depicts the calculated results for the concentration and the orientation fields subjected to the two-wave interference geometries for the content of 35/65 photopolymerized at 30 °C. The rest of the parameters remain unchanged as in the previous case of Figure 3. The structures formed in the 35/65 sample are initially uniform (1000 time steps). In the concentration field, at approximately 2000 time steps and beyond, the LC droplets tend to form an alternating droplet arrays in the low intensity regions of light. In each array, LC droplets form along the layer direction. In the high intensity region of light, liquid crystal molecules are largely trapped in the polymer network before they have a chance to diffuse out. In the orientation field, nematic ordering occurs within the droplets, and thus the emergence of droplets is suggestive of the liquid crystal-rich domains.

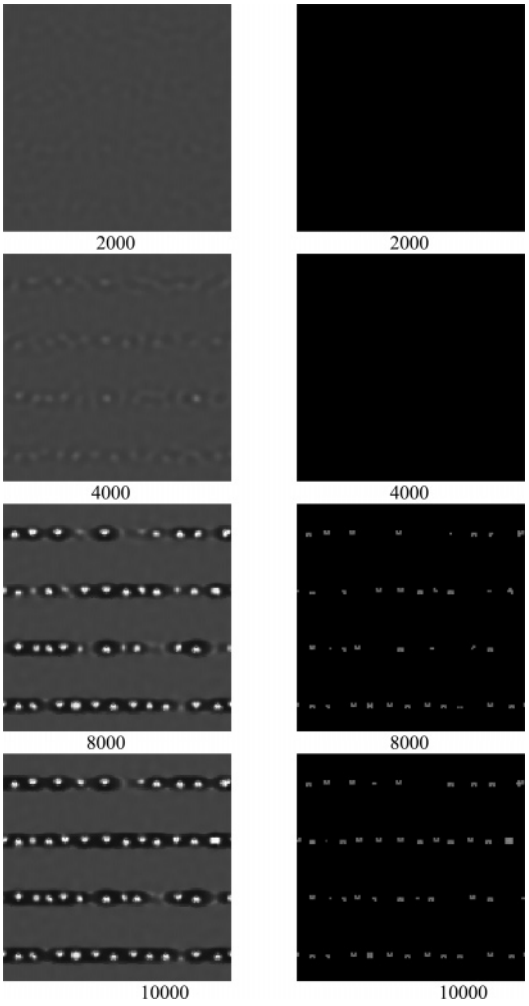

Figure 4. Simulated spatiotemporal growth of concentration order parameter (left array), and orientation order parameter (right array) under uniform photopolymerization for liquid crystal and photoreactive monomer mixed at 35/65.

The temporal evolution of the Fourier transform patterns of the concentration field has been examined in Figure 4. The Fourier results are shown in Figure 5 (left column). At the early time steps from 2000 to 4000, a scattering halo can be recognized without any discernible diffraction spots. However, the scattering halo becomes fuzzy around 8000 time steps, with concurrent emergence of the diffraction peaks in the vertical direction. With elapsed time, the scattering halo is suppressed while the diffraction spots intensify.

To closely examine at the diffraction peaks of the Fourier transform patterns in Figure 5, we sliced the diffraction peaks from the center, cutting through the vertical direction (perpendicular to the stripes) of the patterns. As can be noticed in the FFT images of the emerged structure at 2000 time steps in Figure 5 (right column), the scattering peaks are initially small in magnitude and exhibit nonuniformity. This suggests that the initial scattering patterns seem to be primarily dominated by the interparticle interference of the phase separated domains. From 4000 time steps and onward, the diffraction pattern gradually evolves into the well-defined peaks while the intensity increases noticeably, indicating a grating formation in the concentration field. A notable feature is that the maximum intensity peak positions move from the edge to the center, while the intensity of the outside peaks is diminished.

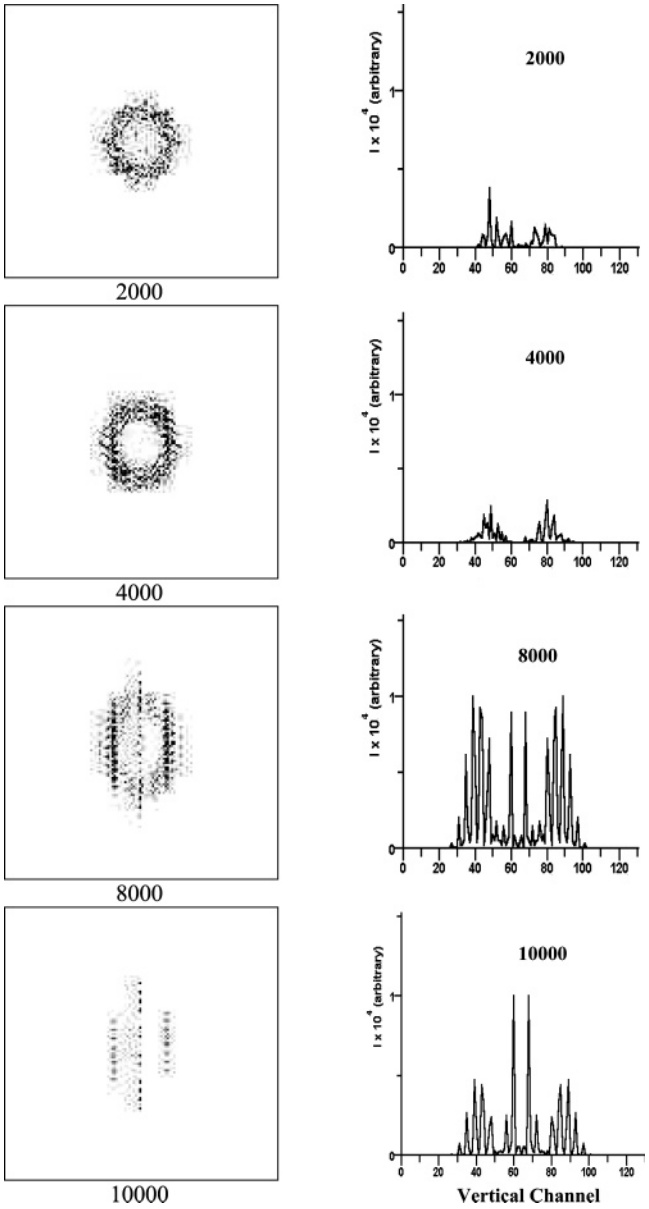

Figure 5. Simulated spatiotemporal growth of Fourier transform patterns (left array) and corresponding one-dimensional vertical slice of diffraction peaks evolution of Fourier transform patterns under two-wave interference pattern photopolymerization for liquid crystal and photoreactive monomer mixed at 35/65.

When LC content is further reduced from 35/65 to 5/95 while all other parameters are kept the same, the system remains in the single phase thermodynamically even after the photopolymerization (see Figure 2b). For such a single-phase system, a single well potential is adequate in describing its physical state, which has only one free energy minimum on a free energy-concentration curve. The most general single well potential is of the Landau type, written as[21]

$$g(\phi_m) = \frac{r}{2}\phi_m{}^2 + \frac{u}{4}\phi_m{}^4 \qquad (15)$$

The signs of r and u must be both positive to yield a single well potential. Alternatively, a single well potential can be obtained by omitting the fourth-order concentration term in eq 15 and setting r to unity. Substituting $g(\phi_m) = \phi_m{}^2/2$, representing the single well

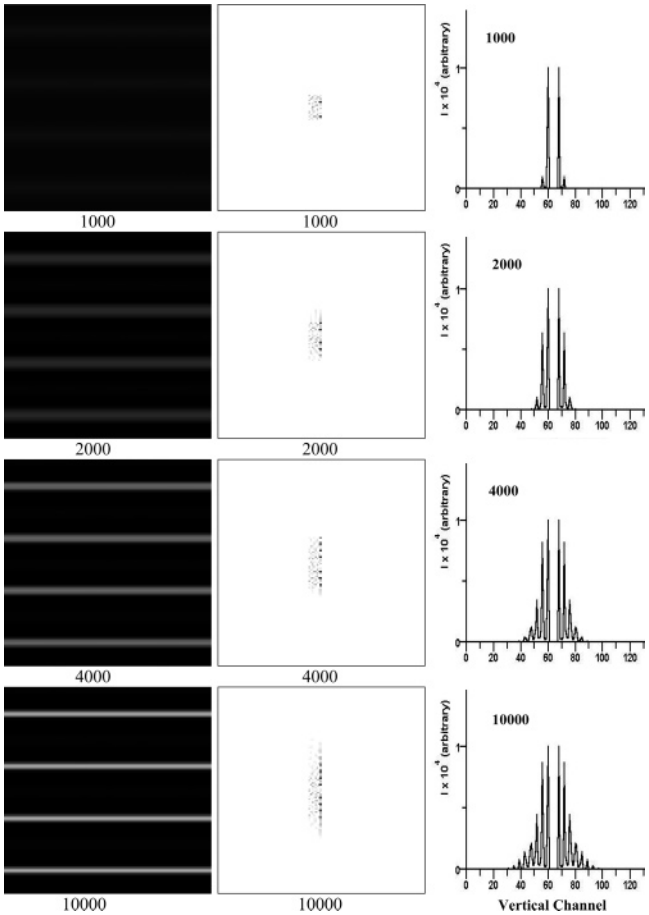

Figure 6. Simulated spatioemporal growth of concentraion order parameter (left array), and Fourier transform patterns (middle array) corresponding one-dimensional vertical slice of diffraction peaks evolution of Fourier transform patterns for the 5/95 composition (right array).

potential, into the TDGL equation in combination with the pattern photoreaction, one obtains

$$\frac{\partial\phi_m(r,t)}{\partial t} = \nabla[\Lambda_m\nabla\phi_m] - k\left[1 + v\cos\left(\frac{2\pi x}{\lambda}\right)\right]\phi_m \qquad (16)$$

which is exactly the classical reaction−diffusion equation for the photopatterning via photopolymerization. In view of the single well potential utilized, the applicability of the conventional reaction−diffusion equation would be limited to a single phase system. Thus, the emerged interference striation structures are governed purely by the transport rather than by thermodynamic criteria. When Λ_m in eq 16 is simplified to the translational diffusivity of the pure monomer, D_m, eq 16 can be deduced to the classical reaction−diffusion equation in one dimension:

$$\frac{\partial\phi_m(r,t)}{\partial t} = D_m\frac{\partial^2\phi_m}{\partial x^2} - k\left[1 + v\cos\left(\frac{2\pi x}{\lambda}\right)\right]\phi_m \qquad (17)$$

Without the second term on the right-hand side of eq 17 is generally known as Fick's equation.[22]

Together with the anisotropic free energy of nematic ordering, the coarse-grain simulation was performed. The results of the evolving concentration fields and Fourier transform patterns of the 5/95 LC content are displayed in Figure 6, right and middle column, respectively. The concentration field shows a regulated LC

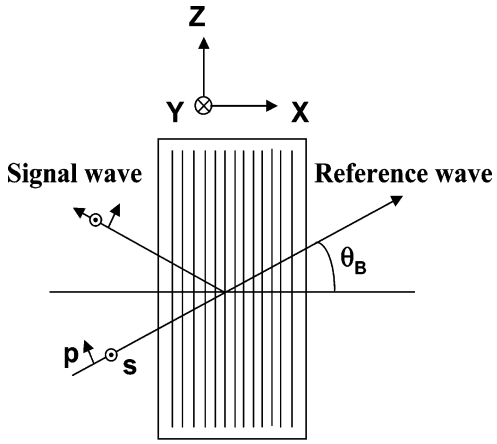

Figure 7. Schematic illustration of reference wave and signal wave in a reflective grating.

stripe formation. In the Fourier transform patterns of the related concentration field, the diffraction spots are sharp and clean because of noninvolvement of the contribution from the phase separation process. In this situation, no liquid crystal ordering is observable in the orientation field. This may be a consequence of the fact that LC content is too low for nematic ordering to take place even in the liquid-crystal-rich region; i.e., the director orientational order parameter is still less than the threshold value for the nematic ordering. Hence, thermodynamics of nematic ordering makes no contribution to this case; that is to say, the patterning process is driven exclusively by materials transport. This is the situation for which the expression of the classical reaction−diffusion equation would be adequate.

In a one-dimensional vertical slice of the diffraction peaks of Figure 6 (right column), as exemplified by the structure formation in the single-phase region, the peaks are symmetric throughout the formation. At later time steps, higher order peaks can be discerned. It is worth mentioning that a similar phenomenon was observed both theoretical and experimentally in the single-component system.[23] The occurrence of higher order peaks was explained in terms of the transformation of the bulk concentration profiles from sinusoidal to nonsinusoidal ones, which is consistent with the single-phase system.

Regarding the gratings formed in Figures 4 and 5, it is challenging to make qualitative predictions of the DE progression, a key property in electrooptical applications of H-PDLC materials. The diffraction efficiency of an ideal, unslanted, and anisotropic reflection grating was extended from the original coupled wave theory,[24] illustrated in Figure 7 and given in the form of[25, 26]

$$\eta = \tanh^2\left(\frac{\pi \Delta n_j(t) l}{\lambda \cos \theta_B}\right) \quad (j = \mathrm{s, p}) \tag{18}$$

where l is the sample thickness, λ is the wavelength of probe light, θ_B is the Bragg angle, and $\Delta n_j(t)$ is the refractive index contrast. For s-polarization $\Delta n_s(t) = n_{a,yy}^{(1)}(t) - n_{a,yy}^{(1)}(0)$, and for p-polarization $\Delta n_p(t) = n_{a,zz}^{(1)}(t) \cos(2\theta_B) + [n_{a,zz}^{(1)}(t) - n_{a,xx}^{(1)}(t)]\sin^2 \theta_B$. The detailed derivation may be found in Appendix A. Further, $n_{a,ii}^{(1)} = \epsilon_{a,ii}^{(1)}/2\epsilon_0 n_i$ ($i = x, y, z$), where n_i is the average refractive index along the i direction, ϵ_0 is the electric permittivity of free space, and ϵ_{ii} are the diagonal components of the dielectric tensor.

$$\epsilon_{a,xx} = \epsilon_{a,yy} = \phi_m \epsilon_m + \phi_p \epsilon_p + \phi_{LC} \epsilon_{\perp x} \tag{19a}$$

$$\epsilon_{a,zz} = \phi_m \epsilon_m + \phi_p \epsilon_p + \phi_{LC} \epsilon_{||} \tag{19b}$$

where

$$\epsilon_{\perp x}/\epsilon_0 = \{n_o^2(s + 2)/3 + n_e^2(1 - s)/3\}(2s + 1)/3 + (n_e^2/3 + 2n_o^2/3)(2 - 2s)/3 \tag{20a}$$

and

$$\epsilon_{||}/\epsilon_0 = \{n_e^2(2s + 1)/3 + n_0^2(2 - 2s)/3\}(2s + 1)/3 + (n_e^2/3 + 2n_o^2/3)(2 - 2s)/3 \tag{20b}$$

The detailed derivation of eqs 20a and 20b may be found in Appendix B. ϵ_m and ϵ_p are the dielectric constants of monomer and polymer, respectively. n_o and n_e refer to the ordinary and extraordinary refractive indices of the liquid crystal. Here ϕ_m, ϕ_p, and ϕ_{LC} are the average volume fraction of monomer, polymer, and liquid crystal in each grating, respectively. In this study, the refractive indices of monomer and polymer are considered to be of the same value (≈1.49), and the refractive indices of the E7 liquid crystals are $n_o = 1.53$ and $n_e = 1.75$, and $l = 8$ μm, $\lambda = 532$ nm, and $\theta_B = 45°$ according to the experimental conditions.

To calculate DE, one of the restrictions is that eq 18 is applicable to gratings with homogeneous stripes in the process of photopatterning. If there are local phase separated structures inside the stripe and if the average length scales are comparable to or larger than the wavelength of light, scattering from these structures will occur due to the interparticle interference effect (see Figure 5). Evidently, such scattering loss cannot be accounted for by eq 18.

To resolve the aforementioned problems, an alternative means is to perform the Fourier transform of the concentration and/or orientation field in two dimensions. The diffraction peaks are inherently related to the statistical average of the local refractive index modulation via Fourier inversion. By definition, the ratio of the combined diffraction peak intensities over the overall scattering and diffraction intensities renders the actual portion of diffraction gratings, δ_a. Hence, the DE for a nonhomogeneous reflection grating can be given in a modified form of eq 18 as

$$\eta = \delta_a \tanh^2\left(\frac{\pi \Delta n_j(t) l}{\lambda \cos \theta_B}\right) \quad (j = \mathrm{s, p}) \tag{21}$$

where the value of $\Delta n_j(t)$, a global parameter, can be retrieved by taking average values of the local refractive indices of the nematic phase in each stripes. Experimentally, it is customary to monitor the change of the first-order diffraction peak which is incapable of distinguishing the sinusoidal from nonsinusoidal concentration shapes. However, the higher order diffraction peak may be used to probe the transformation of sinusoidal to nonsinusoidal profiles.[23] By virtue of its capability for mimicking the nonsinusoidal forms and the interparticle interference scattering from the internal structural heterogeneity inside the stripe, the DE calculation based on the eq 21 turns out to be more rigorous. The DE calculations presented hereafter, unless otherwise specified, are all obtained by this approach.

The calculated DE values are plotted in Figure 8. In the 50% LC mixture, as a result of the scattering from

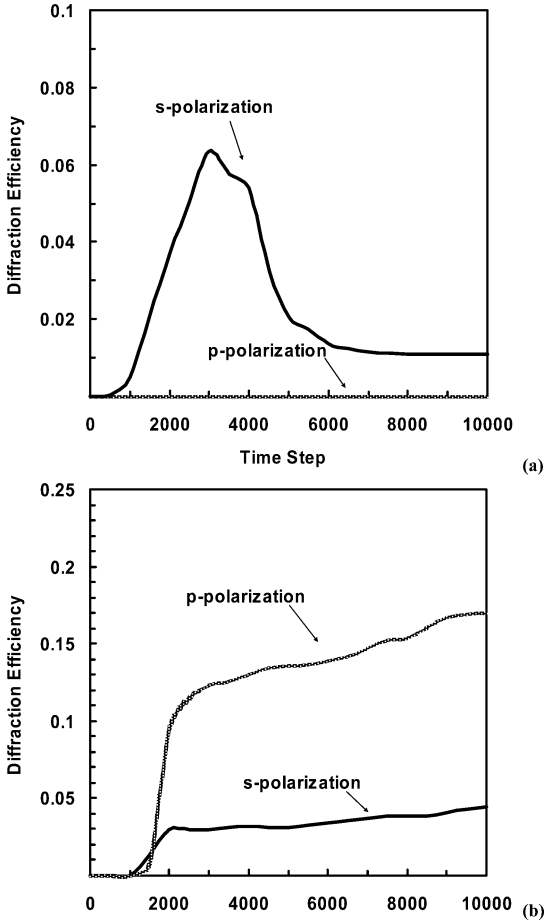

Figure 8. Comparison of diffraction efficiency evolution (s- and p-polarization) of H-PDLC gratings formed under 5/95 (a) and 50/50 LC/monomer composition (b).

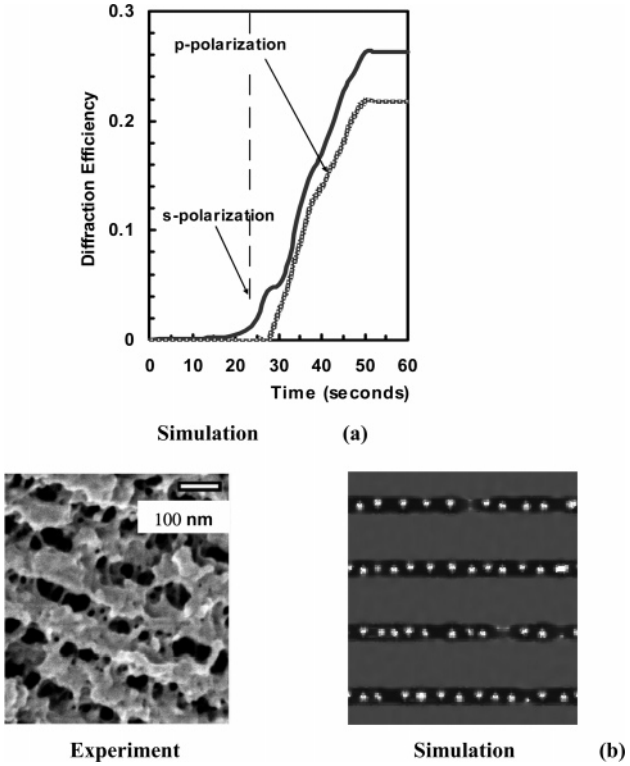

Figure 9. Simulated diffraction efficiency evolution (s- and p-polarization) from 35% LC mixture (a) converted to the real time scale and comparison of experimental reflecting H-PDLC pattern (left) from SEM with the simulated one from 35% LC mixture (b).

the interdomain droplets, the s-polarized DE slowly rises up and eventually settles at a very low level. In contrast, the s-polarized DE of the 5% LC mixture jumps to 7% within 3000 time steps and then levels off. Apparently, the one formed with 5% LC has no heterogeneous stripes in gratings since it is formed in the single phase and consequently a larger s-polarized DE than that of 50% LC. On the other hand, the 5% LC mixture reveals no p-polarization. This observation is understandable because the 5% LC content, though concentrated in the LC rich stripes, may fall below the threshold value for the nematic ordering to take place. Technically, the H-PDLC films formed in the 5% LC sample cannot be switched by an external electric field due to the absence of nematic domains.

It has to be mentioned that the apparent reaction kinetic constant in this paper was initially treated as a constant for simplicity. However, as evidenced in the P-DSC/FTIR experiments, the measured apparent reaction kinetic constant actually changes as a function of time.[29] It should be more realistic to treat the reaction rate constant to be time dependent. After taking into account this time-decaying reaction kinetic constant in our simulation, we have found a similar trend in Figure 8a to what has been observed in the experiment for the 5% LC sample.[30] The effect of time dependence of apparent reaction kinetic constant is especially pronounced when there is more monomer content in the mixture such as 5% LC sample. In contrast, the aforementioned effect is not significant since the reaction rate constant varies very little with time in the higher LC content samples (i.e., 35% LC or 50% LC).

Another noteworthy feature in Figure 8 arises from the comparison of p-polarized DE between the 50% and 5% LC mixtures. Initially, p-polarized DE of the 50% LC mixture is under-developed until 1500 time steps. Afterward, the p-polarized DE emerges and asymptotically saturates out to the final stage, signifying the development of an anisotropic grating. Bearing in mind that the 50% mixture is rich in LC, it can expected that the 50% LC mixture exhibits a higher p-polarized DE than the 5% LC mixture. According to the theoretical predictions mentioned above, the DE of the 5% and 50% mixtures both reflect inferior performance in either s- or p-polarized DE, which is not suitable in the fabrication of H-PDLC. It may be speculated that the optimal LC composition should be somewhere between 5% and 50%.

Figure 9a presents a simulated DE evolution from a 35% LC mixture. We compared Figure 9a with an experimentally monitored DE evolution published in an earlier paper.[27] The experimental result was obtained from a mixture of 35% liquid crystal (BL series from Merck) with monomer diapentaerythol hydroxyl pentacrylate (Aldrich) with a formulation similar to that previously disclosed.[28] The time steps in the simulation were converted to the real time (~50 s) for the evaluation on an equivalent scale. Evidently, there are generally two zones in the development of the DE of the s-polarization. In the first zone, the p-polarization shows no development of the diffraction efficiency. The p-polarized DE starts at the end of the first zone and levels off at the comparable time frame of that of the s-polarization. It is striking that our simulation qualitatively captures the trends of experimental results. All in all, the 35% LC mixture yields the optimum DE

performance among all compositions investigated, which is in good accord with the finding that 35% of LC is a preferred composition for use in the laboratory fabrication of H-PDLC.

Figure 9b demonstrates the comparison between the simulated pattern and the scanning electron microscopy micrograph of experimentally formed H-PDLC. The experimental result was obtained from a mixture of 35% liquid crystal (BL series from Merck) with monomer diapentaerythol hydroxyl pentacrylate (Aldrich) with a formulation similar to that previously disclosed.[29] For the comparison of experimental and simulated droplet sizes, the length scale of simulated LC domain requires estimation via the relationship $t' = (D_c/l_c^2)t$ and $k' = (l_c^2/D_c)k$ with t' and k' the dimensionless time and apparent reaction kinetic constant and D_c the characteristic diffusion coefficient. In practice, the translational diffusion coefficient of acrylic monomer is around $\sim 10^{-10}$ cm^2/s, and the diffusion coefficient of liquid crystal is about $\sim 10^{-8}$cm^2/s. In this paper, D_m and D_{LC} are taken as $D_m = 0.01$ and $D_{LC} = 2$ so that the resulting characteristic diffusion coefficient of LC/monomer system is close to 10^{-8} cm^2/s. The experimental exposure time is about 20−30 s, and the simulated time is approximately 10^4 time steps. Thus, the characteristic length l_c is roughly in the range of 40−50 nm, and the average sizes of the simulated liquid crystal domains are approximately a few hundred nanometers, which is in the comparable range of the experimental ones. The striking similarity between the morphological patterns and the DE behavior of the theoretical calculation and the experiment is quite promising.

Summary

Pattern photopolymerization in mixtures of liquid crystal and photoreactive monomer was simulated in the context of the time-dependent Ginzburg−Landau equations (model C) coupled with photopolymerization reaction kinetics in the various phase regions. Distinct morphology was found in each phase region. Of particular interest is that when the system remains in the single-phase region throughout the photopolymerization, the formed patterns revealed no phase-separated structure. The absence of internal heterogeneity improves in eliminating the scattering halo while intensifying the diffraction peaks, and thus a significant improvement can be made in the s-polarized diffraction efficiency. A further step was taken to qualitatively predict the behavior of the diffraction efficiency by means of the 2-D FFT approach by taking into consideration the contribution from the interparticle interference scattering from the internal structural heterogeneity within the stripe layers. On the basis of the aforementioned theoretical calculations, the 35/65 LC sample had the optimum overall diffraction efficiency from both s- and p-polarization viewpoints. A comparison between the theoretical predictions and experimental findings showed a remarkable consistency.

Acknowledgment. Support from the National Science Foundation through Grant DMR 02-09272, the Collaborative Center for Polymer Photonics, sponsored by Air Force Office of Scientific Research, Wright-Patterson Air Force Base, and University of Akron, Akron Global Polymer Academy, and Ohio Board of Regents Research Challenge Grant has been gratefully acknowledged.

Appendix A. Derivation of the Dielectric Tensor

The expression for the dielectric tensor ϵ used in the coupled-wave theory is

$$\epsilon(x) = \epsilon^{(0)} + \epsilon^{(1)} \cos(Kx) \tag{A-1}$$

where $K = 2\pi N_x/L$. In eq A-1, $\epsilon^{(0)}$ is the space-averaged part of the dielectric tensor and $\epsilon^{(1)}$ is the first Fourier component of the dielectric tensor modulation. To obtain an expression for $\epsilon^{(1)}$, one must model the dielectric tensor distribution of the HPDLC. Since the grating is formed as LC-rich and polymer-rich strips, we can write this as

$$\epsilon(x) = \begin{cases} \epsilon_a & \text{LC-rich stripe} \\ \epsilon_b & \text{polymer-rich stripe} \end{cases} \tag{A-2}$$

In reality, ϵ_a and ϵ_b are nonuniform inside each stripe. But, we may treat them as uniform for simplicity. To obtain the modulation in the form of eq A-2, eq A-2 is examined by Fourier analysis. We can do this by expanding eq A-2 in a Fourier cosine series:

$$\epsilon(x) = \sum_{n=0}^{\infty} \epsilon^{(n)} \cos(nKx) \tag{A-3}$$

If we let α_r be the fraction of the grating period occupied by the LC rich stripe, then

$$\epsilon^{(0)} = \alpha_r \epsilon_a + (1 - \alpha_r)\epsilon_b \tag{A-4}$$

$$\epsilon^{(1)} = \frac{2}{\pi} \sin(\alpha\pi)(\epsilon_a - \epsilon_b) \tag{A-5}$$

For the polymer stripe, we can take

$$\epsilon_{b,ij} = (\epsilon_m \phi_m + \epsilon_p \phi_p + \epsilon_i \phi_{LC})_{polymer} \delta_{ij} \tag{A-6a}$$

where ϵ_m and ϵ_p are the dielectric constants of the monomer and polymer, respectively, and ϵ_i is the isotropic value of the LC dielectric constant. ϕ_m, ϕ_p, and ϕ_{LC} are the respective average volume fractions of monomer, polymer, and LC in the polymer strip at initial time.

In the photopolymerization, the photoreaction is so fast that we assume that LCs in the highest intensity region are immediately trapped due to cross-linking before they can diffuse away. Hence, the ϵ value in the polymer stripe does not change as a function of time.

Also, the volume fractions of monomer, polymer, and LC in the high intensity region and low intensity region are apparently the same at initial time. Therefore, eq A-6a can be expressed as

$$\epsilon_{a,ii} = \epsilon_{b,ii} = (\epsilon_m \phi_m + \epsilon_p \phi_p + \epsilon_i \phi_{LC})_{LC} \quad (\text{at time} = 0,\ i = x, y, z) \tag{A-6b}$$

For the LC stripe

$$\epsilon_{a,xx} = \epsilon_{a,yy} = (\epsilon_m \phi_m + \epsilon_p \phi_p + \epsilon_{\perp x} \phi_{LC})_{LC} \tag{A-7a}$$

$$\epsilon_{a,zz} = (\epsilon_m \phi_m + \epsilon_p \phi_p + \epsilon_{||} \phi_{LC})_{LC} \tag{A-7b}$$

ϕ_m, ϕ_p, and ϕ_{LC} are the volume fractions of monomer, polymer, and liquid crystal in the PDLC stripe at any given time, respectively.

DE in terms of an index modulation takes the form of

$$\Delta n_s(t) = \frac{\epsilon_{a,yy}(t) - \epsilon_{a,yy}(0)}{2\epsilon_0 n_y(t)} \quad \text{(A-8)}$$

where $n_y(t) = (\epsilon_{a,yy}(t)/\epsilon_0)^{1/2}$.

For p-polarization

$$\Delta n_p(t) = \frac{[\epsilon_{a,zz}(t) - \epsilon_{a,zz}(0)]\cos^2\theta - [\epsilon_{a,xx}(t) - \epsilon_{a,xx}(0)]\sin^2\theta}{2\epsilon_0 n(\theta,t)} \quad \text{(A-9)}$$

For a weakly birefringent medium, which is typically the case, $n_x \approx n_z \approx n_y \equiv n$. Also then, for any θ, $n(\theta) \approx n$.

Appendix B. Derivation of the Dielectric Components $\epsilon_\perp$, $\epsilon_\parallel$ of Liquid Crystal

Orientation order parameter s takes the form of

$$s = \frac{3\langle\cos^2\theta\rangle - 1}{2} \quad \text{(B-1)}$$

where $\langle\cos^2\theta\rangle$ is the ensemble average of all director orientations in respect to the reference axis (Z axis). θ is defined as the angle between the LC director and the reference axis. The orientational order parameter s can be linked to experimentally measurable quantities via Lorentz−Lorenz type equations for the nematic phase:[31−33]

$$(n_e^2 - 1)/(\bar{n}^2 + 2) = \frac{N}{3\epsilon_0}\left(\bar{\alpha} + \frac{2}{3}s\Delta\alpha\right) \quad \text{(B-2)}$$

and

$$(n_o^2 - 1)/(\bar{n}^2 + 2) = \frac{N}{3\epsilon_0}\left(\bar{\alpha} - \frac{1}{3}s\Delta\alpha\right) \quad \text{(B-3)}$$

where n_e and n_o are the extraordinary and ordinary refractive indices of the nematic medium with $\bar{n} = {}^1/_3 n_e^2 + {}^2/_3 n_o^2$, $\bar{\alpha} = {}^1/_3(\alpha_e + 2\alpha_o)$, $\Delta\alpha = \alpha_e - \alpha_o$, and N is the number of molecules per unit volume. α_e and α_o represent the extraordinary and ordinary polarizabilities of LC molecules, respectively.

It should be emphasized in eqs B-2 and B-3 that n_e and n_o are the properties of the bulk liquid crystal while α_e and α_o are the properties of the LC molecules. When $s = 1$, n_e^2 and n_o^2 are directly proportional to α_e and α_o.

Now, $n_\parallel$, the refractive index of LC parallel to the reference Z axis in bulk may be described in the form of

$$n_\parallel^2 = n_e^2\langle\cos^2\theta\rangle + n_o^2\langle\sin^2\theta\rangle \quad \text{(B-4)}$$

Similarly, $n_{\perp x}$ or $n_{\perp y}$, the refractive index of LC along x or y axis, perpendicular to the reference axis (see Figure 9) may be written in the form of

$$n_{\perp y}^2 = n_{\perp x}^2 = n_o^2\langle\cos^2\theta\rangle/2 + n_o^2/2 + n_e^2\langle\sin^2\theta\rangle/2 \quad \text{(B-5)}$$

By virtue of the uniaxial symmetry consideration in the Maier−Saupe theory, the probability of the n_e^2 or n_o^2 projection preferentially aligning along the x- or y-axis is equivalent. In practice, the LC directors by no means align perfectly along the Z axis in the nematic phase, and thus both eqs B-4 and B-5 may be modified as

$$n_\parallel^2 = \{n_e^2\langle\cos^2\theta\rangle + n_o^2\langle\sin^2\theta\rangle\}\langle\cos^2\theta\rangle + (1 - \langle\cos^2\theta\rangle)\left(\frac{1}{3}n_e^2 + \frac{2}{3}n_o^2\right) \quad \text{(B-6)}$$

$$n_{\perp x}^2 = n_{\perp y}^2 = \left\{n_o^2\frac{\langle\cos^2\theta\rangle + 1}{2} + n_e^2\frac{\langle\sin^2\theta\rangle}{2}\right\}\langle\cos^2\theta\rangle + (1 - \langle\cos^2\theta\rangle)\left(\frac{1}{3}n_e^2 + \frac{2}{3}n_o^2\right) \quad \text{(B-7)}$$

Rearranging the two equations above as a function of s, one gets

$$n_\parallel^2 = \{n_e^2(2s + 1)/3 + n_o^2(2 - 2s)/3\}(2s + 1)/3 + (n_e^2/3 + 2n_o^2/3)(2 - 2s)/3 \quad \text{(B-8)}$$

$$n_{\perp x}^2 = n_{\perp y}^2 = \{n_o^2(s + 2)/3 + n_e^2(1 - s)/3\}(2s + 1)/3 + (n_e^2/3 + 2n_o^2/3)(2 - 2s)/3 \quad \text{(B-9)}$$

At optical frequencies, the parallel and perpendicular components of refractive indices can be related to the corresponding components in dielectric constants in what follows:

$$\epsilon_{\perp x}/\epsilon_o = \epsilon_{\perp y}/\epsilon_o = n_{\perp x}^2 \quad \text{and} \quad \epsilon_\parallel/\epsilon_o = n_\parallel^2 \quad \text{(B-10)}$$

which may be linked to eqs 20a and 20b.

References and Notes

(1) Bunning, T. J.; Natarajan, L. V.; Tondiglia, V. P.; Sutherland, R. L.; Vezie, D. L.; Adams, W. W. *Polymer* **1995**, *36*, 2699.
(2) Bowley, C. C.; Crawford, G. P.; Yuan, H. *Appl. Phys. Lett.* **1999**, *21*, 3096.
(3) Tondiglia, V. P.; Natarajan, L. V.; Sutherland, R. L.; Tomlin, D.; Bunning, T. J. *Adv. Mater.* **2002**, *14*, 18.
(4) Jakubiak, R.; Bunning, T. J.; Vaia, R. A.; Natarajan, L. V.; Tondiglia, V. P. *Adv. Mater.* **2003**, *15*, 241.
(5) Yablonovitch, E. *Phys. Rev. Lett.* **1987**, *58*, 2059.
(6) John, S. *Phys. Rev. Lett.* **1987**, *58*, 2486.
(7) Joannopoulous, J. D.; Meade, R. D.; Winn, J. N. *Photonic Crystals*; Princeton University Press: New York, 1995.
(8) Lin, S. Y.; Chow, E.; Hietala, V.; Villeneuve, P. R.; Joannopoulous, J. D. *Science* **1998**, *282*, 274.
(9) Kyu, T.; Nwabunma, D. *Macromolecules* **2001**, *34*, 9168.
(10) Scranton, A. B.; Bowman, C. N.; Peiffer, R. W. *ACS Symp. Ser.* **1996**, *673*.
(11) Bunning, T. J.; Natarajan, L. V.; Tondiglia, V. P.; Dougherty, G.; Sutherland, R. L. *J. Polym. Sci., Part B: Polym. Phys.* **1997**, *35*, 2825.
(12) Sarkar, M. D.; Gill, N. L.; Whitehead, J. B.; Crawford, G. P. *Macromolecules* **2003**, *36*, 630.
(13) Zhao, G. H.; Mouroulis, P. *J. Mod. Opt.* **1994**, *41*, 1929.
(14) van Nostrum, C. F.; Nolte, R. J. M.; Broer, D. J.; Fuhrman, T.; Wendorff, J. H. *Chem. Mater.* **1998**, *10*, 135.
(15) Bowley, C. C.; Crawford, G. P. *Appl. Phys. Lett.* **2000**, *76*, 2235.
(16) Sutherland, R. L.; Tondiglia, V. P.; Natarajan, L. V.; Bunning, T. J. *J. Appl. Phys.* **2004**, *96*, 951.
(17) Flory, P. J. *J. Chem. Phys.* **1942**, *10*, 51.
(18) Huggins, M. L. *J. Phys. Chem.* **1942**, *46*, 151.
(19) Maier, W.; Saupe, A. *Z. Naturforsch., A* **1958**, *13*, 564.
(20) Shen, C.; Kyu, T. *J. Chem. Phys.* **1995**, *102*, 556.
(21) Nwabunma, D.; Chiu, H.-W.; Kyu, T. *J. Chem. Phys.* **2000**, *113*, 6429.
(22) Gunton, J. D.; San Miguel, M.; Sahni, P. S. Academic Press: New York, 1983.
(23) Atkins, P. W. *Physical Chemistry*, 5th ed.; W.H. Freeman and Co.: New York, 1994.
(24) Meng, S.; Kumar, N.; Kyu, T.; Natarajan, L. V.; Tondiglia, V. P.; Bunning, T. J. *Macromolecules* **2004**, *37*, 3792.
(25) Kogelnik, H. *Bell Syst. Technol. J.* **1969**, *48*, 2909.
(26) Montemezzani, G.; Zgonik, M. *Phys. Rev. E* **1997**, *55*, 1035.
(27) Sutherland, R. L. *J. Opt. Soc. Am. B* **2002**, *19*, 2995.
(28) Sutherland, R. L.; Tondiglia, V. P.; Natarajan, L. V.; Bunning, T. J. *Appl. Phys. Lett.* **2001**, *79*, 1420.

(29) Sutherland, R. L.; Natarajan, L. V.; Tondiglia, V. P.; Bunning, T. J. *Chem. Mater.* **1993**, *5*, 1533.
(30) Meng, S. Ph.D. Dissertation, The University of Akron, May 2004.
(31) Meng, S.; Duran, H.; Nanjundiah, K.; Hu, J.; Soucek, M.; Kyu, T.; Sutherland, R. L.; Tondiglia, V. P.; Natarajan, L. V.; Bunning, T. J. Manuscript in preparation.
(32) Chandrasekhar, S.; Madhusudana, N. V. *J. Phys. (Paris), Suppl.* **1969**, *30*, C4-24.
(33) Vuks, M. F. *Opt. Spektrosk.* **1966**, *20*, 644.
(34) Haller, I.; Huggins, H. A.; Lilienthal, H. R.; Mcguire, T. R. *J. Phys. Chem.* **1973**, *77*, 950.

MA0480906